Published in final edited form as:
J Neurochem. 2010 September 1; 114(5): 1436–1446. doi:10.1111/j.1471-4159.2010.06862.x.

ER Ca^{2+} signaling and mitochondrial Cyt *c* release in astrocytes following oxygen and glucose deprivation

Yan Liu[1,4], **Douglas B. Kintner**[2,4], **Gulnaz Begum**[4], **Jehad Algharabli**[4], **Pelin Cengiz**[3], **Gary E. Shull**[5], **Xiang-Jun Liu**[1], and **Dandan Sun**[2,4]

[1] Dept. of Biological Sciences and Biotechnology, School of Medicine, Tsinghua University, Beijing, P.R. China

[2] Dept. of Neurological Surgery, University of Wisconsin School of Medicine and Public Health, Madison, WI 53705, USA

[3] Dept. of Pediatrics, University of Wisconsin School of Medicine and Public Health, Madison, WI 53705, USA

[4] Waisman Center, Madison, WI 53705, USA

[5] Dept. of Molecular Genetics, Biochemistry and Microbiology, University of Cincinnati, Cincinnati, OH 45267, USA

Abstract

In the present study, we investigated changes of cytosolic Ca^{2+} ($[Ca^{2+}]_{cyt}$), endoplasmic reticulum Ca^{2+} ($[Ca^{2+}]_{ER}$), and mitochondrial Ca^{2+}($Ca^{2+}{}_m$) in astrocytes following oxygen/glucose deprivation and reoxygenation (OGD/REOX). Two hours OGD did not cause changes in $[Ca^{2+}]_{cyt}$, but led to a significant increase in $[Ca^{2+}]_{ER}$. The elevation in $[Ca^{2+}]_{ER}$ continued and reached a peak level (130 ± 2 μM) by 90 min REOX. An abrupt release of $Ca^{2+}{}_{ER}$ occurred during 1.5–2.5 h REOX, which was accompanied with a delayed and sustained rise in $[Ca^{2+}]_{cyt}$. Moreover, $Ca^{2+}{}_m$ content was increased significantly within 15 min REOX followed by a secondary rise (~ 4.5-fold) and a release of mitochondrial cytochrome *c* (Cyt *c*). Astrocytes exhibited translocation of Cyt *c* from mitochondria to ER and up regulation of ER stress protein p-eIF2α. Blocking Na^+-K^+-Cl^- cotransporter isoform 1 (NKCC1) activity, either by its potent inhibitor bumetanide or genetic ablation, abolished release of ER Ca^{2+}, delayed rise in $[Ca^{2+}]_{cyt}$ and $Ca^{2+}{}_m$. Inhibition of the reverse mode operation of the Na^+/Ca^{2+} exchanger (NCX_{rev}) significantly attenuated OGD/REOX-mediated Cyt *c* release. In summary, our study illustrates that OGD/REOX triggers a time-dependent loss of Ca^{2+} homeostasis in cytosol and organelles (ER and mitochondria) in astrocytes. Collective stimulation of NKCC1 and NCX_{rev} contributes to these changes.

Keywords

reactive astrocytes; mitochondrial Ca^{2+}; ER Ca^{2+}; ER stress; bumetanide

Address correspondence to: Dandan Sun, M.D., Ph.D., Department of Neurological Surgery, University of Wisconsin Medical School, T513 Waisman Center, 1500 Highland Ave., Madison, WI, 53705, Tel: (608) 263-4060, Fax: (608) 263-1409, sun@neurosurg.wisc.edu.

INTRODUCTION

Cytochrome *c* (Cyt *c*) has been suggested to function as a messenger in coordinating endoplasmatic reticulum (ER) and mitochondrial interactions and in accelerating apoptotic cell death (Boehning et al. 2003). Early in apoptosis, Cyt *c* translocates from mitochondria to ER where it selectively binds to inositol 1,4,5-triphosphate receptor (IP_3R) and triggers sustained, oscillatory cytosolic Ca^{2+} increases, resulting in release of Cyt *c* from all mitochondria (Boehning et al. 2003). This phenomenon has been identified as a feed-forward mechanism that amplifies the apoptotic signals by a coordinated release of ER Ca^{2+} and Cyt *c* (Boehning et al. 2003; Boehning et al. 2004). Coimmunoprecipitation of Cyt *c* and IP_3R type 1 (IP_3R1) and/or ryanodine receptor type 2 (RyR_2) was detected in gerbil hippocampus following transient brain ischemia (Beresewicz et al. 2006), suggesting that a coordinated release of ER Ca^{2+} and Cyt *c* may play a role in ischemic cell damage.

Release of Ca^{2+} from intracellular Ca^{2+} stores is a key component in astrocyte function under physiological conditions. This includes ATP-mediated Ca^{2+} release, which leads to a spatial expansion of astrocyte activation and plays an important role in coordination and synchronization of astrocyte responses to synaptic transmission (Smith et al. 2003; Takano et al. 2009). On the other hand, ER Ca^{2+} stores sequester Ca^{2+} to prevent intracellular Ca^{2+} overload in astrocytes in *in vitro* model of ischemia such as oxygen/glucose deprivation/reoxygenation (OGD/REOX) (Lenart et al. 2004). This event is accompanied with changes in mitochondrial function including increase of mitochondrial Ca^{2+} ($Ca^{2+}{}_m$) and depolarization of mitochondrial membrane potential (Ψ_m) (Kintner et al. 2007). However, the temporal changes in Ca^{2+} homeostasis of ER and mitochondria, as well as in mitochondrial Cyt *c* release are not well studied in astrocytes.

It has been demonstrated that non-NMDA mediated Ca^{2+} influx plays a significant role in astrocyte damage. For example, ischemia-induced astrocyte death depends on extracellular Ca^{2+} and is prevented by inhibition of the reverse mode of the Na^+/Ca^{2+} exchanger (NCX_{rev}) (Bondarenko et al. 2005). Pharmacological inhibition or genetic ablation of Na^+-K^+-Cl^- cotransporter isoform 1 (NKCC1) attenuates $Ca^{2+}{}_m$ overload and Ψ_m depolarization (Kintner et al. 2007). However, it is unknown whether the collective stimulation of NKCC1 and NCX_{rev} plays a role in altering ER and mitochondrial Ca^{2+} signaling and Cyt c release in ischemic astrocytes.

In the present study, we detected changes in $Ca^{2+}{}_{ER}$, $Ca^{2+}{}_m$, $Ca^{2+}{}_{cyt}$ as well as Cyt *c* release in cultured cortical astrocytes following 2 h OGD and 0–180 min REOX. We found that there was a concerted loss of $Ca^{2+}{}_{ER}$, $Ca^{2+}{}_m$, and $Ca^{2+}{}_{cyt}$ homeostasis and release of Cyt *c*. Inhibition of NKCC1 and NCX_{rev} activity significantly reduced mitochondrial and ER dysfunctions in astrocytes following OGD/REOX.

EXPERIMENTAL PROCEDURES

Materials

Eagle's modified essential medium (EMEM) and Hanks balanced salt solution (HBSS) were from Mediatech Cellgro (Manassas, VA). Fetal bovine serum (FBS) was obtained from Valley Biomedical Inc. (Winchester, VA). Collagen-type I was from Collaborative Biomedical Products (Bedford, MA). Bumetanide, carbonyl cyanide-p-trifluoromethoxyphenylhydrazone (FCCP), dibutyryl cyclic AMP (dBcAMP), sodium borohydride, and xestospongin C were purchased from Sigma Chemicals (St. Louis, MO). SEA0400 was a kind gift from Taisho Pharmaceutical Co. Ltd. (Omiya, Saitama, Japan). Fura-2 acetoxymethyl ester (Fura-2 AM), BR-A23187, MitoTracker green, mag-fura-2 AM, TO-PRO-3, and rhod 2-AM were from Invitrogen (Carlsbad, CA). 2-APB was from Tocris

(Ellisville, MO). Mouse anti-Cyt *c* monoclonal antibodies (clone 6H2.B4 for immunofluorescence, clone 7H8.2C12 for western blotting) were purchased from BD Pharmingen (SanDiego, CA). Rabbit anti-MnSOD polyclonal antibody and rabbit anti-Calnexin polyclonal antibody were from Stressgen (Ann Arbor, MI). Rabbit anti-IP_3R1 antiserum was from Millipore (Billerica, MA). Rabbit anti-phospho-eIF2α polyclonal antibody was from Cell Signaling Technology (Danvers, MA). Mouse anti-GFAP monoclonal antibody was from Sternberger Monoclonals (Lutherville, MD). Rabbit anti-Actin polyclonal antibody was from Santa Cruz Biotechnology (Santa Cruz, CA) Pluronic F-127 was from BASF Corp (Parsippany, NJ).

Animals and genotype analysis

NKCC1 homozygous mutant and wild-type mice (129/SvJ Black Swiss) were obtained by breeding gene-targeted NKCC1 heterozygous mutant mice (Flagella et al. 1999), and genotypeswere determined by polymerase chain reaction (PCR) analysis of DNA fromtail biopsies as described previously (Su et al. 2002)

Primary culture of mouse cortical astrocytes

Dissociated cortical astrocyte cultures were established as described before (Su et al. 2002). Cerebral cortices were removed from 1-day-old $NKCC1^{+/+}$ or $NKCC1^{-/-}$ mice. The cortices were incubated in a trypsin solution (0.25 mg/ml of HBSS) for 25 min at 37°C. The dissociated cells were rinsed and resuspended in EMEM containing 10% FBS. Viable cells (1×10^4 cells/well) were plated in petri dishes (100 × 20 mm) or on glass coverslips (22 × 22 mm) in 6-well plates coated with collagen type-1. Cultures were maintained in a 5% CO_2 atmosphere at 37°C and refed every 3 days throughout the study. To obtain morphologically differentiated astrocytes, confluent cultures (7 days in culture, DIV 7) were treated with EMEM containing 0.25 mM dBcAMP to induce differentiation. dBcAMP has been widely used to mimic neuronal influences on astrocyte differentiation (Swanson et al. 1997). Experiments were routinely performed in DIV 10–21 cultures.

OGD treatment

$NKCC1^{+/+}$ or $NKCC1^{-/-}$ astrocytes on coverslips were rinsed twice with an isotonic OGD solution (pH 7.4) containing (in mM, at 37°C): 0 glucose, 26 $NaHCO_3$, 120 NaCl, 5.36 KCl, 0.33 Na_2HPO_4, 0.44 KH_2PO4, 1.27 $CaCl_2$, 0.81 $MgSO_4$. Cells were incubated in 1 ml of the OGD solution in a hypoxic incubator for 2 h (Forma Scientific Inc, model 3130, Marietta, OH), containing 94% N_2, 1% O_2 and 5% CO_2. An orbital shaker (Thermolyne Inc, model M48215, Dubuque, IA) in the hypoxic chamber was used to facilitate equilibration of the hypoxic gases during the initial 30 min OGD. Normoxic control cells were incubated in 5% CO_2 and atmospheric air for 2 h in a control HCO_3^--MEM buffer containing 5.5 mM glucose. For REOX, OGD-treated cells were incubated with the HCO_3^--MEM buffer under conditions identical to the normoxic controls. Cells grown in petri dishes were treated similarly as described above, except the solution volumes were 5 ml.

Cytosolic Ca^{2+} ($[Ca^{2+}]_{cyt}$) measurement

Astrocytes grown on coverslips were incubated with 5 μM fura-2 AM during 2 h OGD at 37°C (Lenart et al. 2004). For REOX, the coverslip was quickly (< 2 min) placed on an open-bath imaging chamber and superfused (1 ml/min) with HCO_3^--MEM at 37° C. Using a Nikon TE 300 inverted epifluorescence microscope (40X oil immersion objective lens), astrocytes were excited every 5 min at 340 and 380 nm and the emission fluorescence at 510 nm recorded. Images were collected and analyzed with the MetaFluor (Molecular Devices, Sunnyvale, CA) image-processing software. At the end of each experiment, the cells were exposed to 1 mM $MnCl_2$ and 5 μM BR-A23187 in Ca^{2+}-free HEPES-MEM. The Ca^{2+}

insensitive fluorescence was subtracted from each wavelength before calculations (Lenart et al. 2004). The $MnCl_2$-corrected 340/380 emission ratios were converted to cytosolic Ca^{2+} concentration ($[Ca^{2+}]_{cyt}$) as described previously (Lenart et al. 2004).

ER Ca^{2+} ($[Ca^{2+}]_{ER}$) measurement

Astrocytes on coverslips were incubated with 4 μM mag-fura-2 AM and 0.02 % pluronic acid during 2 h OGD. In a previous study, we validated the selective determination of $[Ca^{2+}]_{ER}$ by mag-fura-2 AM (Chen et al. 2008). The coverslip was placed on an open-bath imaging chamber in HEPES-MEM at 37°C. Cells were excited every 10 sec at 345 and 385 nm and the emission fluorescence images collected at 510 nm using Nikon TE 300 inverted epifluorescence microscope (40X objective lens). The $Ca^{2+}{}_{ER}$ values were calculated using the equation $[Ca^{2+}_{ER}]=K\times(R_{base}-R_{\min})/(R_{\max}-R_{base})$. K was determined as 72 μM in astrocytes using solutions of known Ca^{2+} concentrations (Calcium Calibration Buffer Kit, Invitrogen, Carlsbad, CA). R_{min} was obtained from a minimum $F_{345/385}$ ratio in a Ca^{2+}-free solution. R_{max} was the maximum $F_{345/385}$ ratio in a high Ca^{2+} solution (10 mM $CaCl_2$).

Measurement of mitochondrial Ca^{2+} ($Ca^{2+}{}_m$)

Astrocytes on coverslips were incubated at 37°C for 60 min with 200 nM MitoTracker green and 9 μM rhod2-AM which was reduced in the presence of a minimum of sodium borohydride and 3 mM sodium succinate in HCO_3^- MEM (Marks et al. 2005; Kintner et al. 2007). Coverslips were placed in the perfusion chamber on the stage of the Leica DMIRE2 confocal microscope and superfused (1 ml/min) with HCO_3^--MEM at 37° C. Cells (1–3 in the field) were visualized with a 60X oil-immersion objective and scanned sequentially for MitoTracker green (ex. 488 nm argon laser line, em. 500–545 nm) and rhod-2 (ex. 543 HeNe laser, em 544–677). The MitoTracker green signal was used to maintain focus prior to each sequential scan. Sequential scans were analyzed using the Leica confocal software. Average grayscale values were collected from regions of interest around mitochondrial clusters exhibiting colocalization of MitoTracker green and rhod-2. $Ca^{2+}{}_m$ values were expressed as relative change of rhod-2 signals from the baseline values and summarized data represent the average of the calculated values from 7–10 cells/experiment as described before (Kintner et al. 2007).

Cyt c immunofluorescence staining

Cyt *c* release from mitochondria was determined by double staining of cells with specific antibody against Cyt *c* and specific antibody against mitochondrial protein manganese superoxide dismutase (MnSOD). Briefly, cells on coverslips were fixed in 4% paraformaldehyde in PBS for 15 min. After rinsing, cells were incubated with blocking buffer (10% normal goat serum, 0.4% Triton X-100 and 0.5% BSA in PBS) for 20 min followed by application of anti-Cyt *c* antibody (1:100 diluted in the blocking buffer) and anti-MnSOD antibody (1:50 diluted in the blocking buffer) for 1 h at 37°C. After rinsing in PBS, cells were incubated with goat anti-mouse secondary antibody IgG (H+L) conjugated to Alexa Fluor® 488 (1:200 dilution) and goat anti-rabbit secondary antibody IgG (H+L) conjugated to Alexa Fluor® 546 (1:200 dilution) for 1 h at 37°C. Nuclei were stained with TO-PRO-3 (1:1000 diluted in PBS) for 15 min at 37°C. Using the Leica DMIRE2 inverted confocal laser-scanning microscope, samples were excited at 488 nm (argon/krypton), 543 nm, and 633 nm and the emission fluorescence was recorded at 512–548 nm, 585–650 nm, or 650–750 nm, respectively. A single optical section of the cells was obtained with a 100X lens and Leica confocal software.

Quantitative analysis of the Cyt c release

Cyt *c* release from mitochondria was quantified by its co-localization with the mitochondrial protein MnSOD using Image J software (NIH, Bethesda, MD) with the Image J plug-in JACoP. An estimate of the colocalization events between both images was obtained by calculating the Pearson's coefficient (Rp) (Bolte and Cordelieres 2006) and Manders' coefficient (M2) (Manders et al. 1992). The Pearson's coefficient is a global statistical approach that performs intensity correlation coefficient-based analysis with an Rp value ranging from 1 to −1 (1: complete positive correlation, −1: negative correlation, zero: no correlation). Manders' coefficients (M1 and M2) are based on the Pearson's correlation coefficient with average intensity values being taken out of the mathematical expression (Manders et al. 1992). Manders' coefficients vary from 0 (non-overlapping) to 1 (100% co-localization). M2 is defined as the ratio of the "summed intensities of pixels from the MnSOD red image for which the intensity in the green channel is above zero" to the "total intensity in the red channel"(Manders et al. 1992). Therefore, M2 is a good indicator of the proportion of the red signal coincident with a signal in the green channel over its total intensity. For quantitative analysis, single optical sections were taken randomly from 5–7 different regions on each coverslip and 5 cells were analyzed from each optical section. The data were obtained from 3–6 independent cultures (n = 3–6).

Subcellular fractionation

Cells were harvested by gently scraping plates with a cell scraper and washing once with ice-cold PBS. The cell pellets were resuspended in 1 ml ice cold buffer A [250 mM sucrose, 10 mM Tris-HCl at pH 7.5, 1 mM EGTA and protease inhibitors, as described previously (Sun et al. 1995)]. Cells were then homogenized on ice using a 1-ml glass Dounce homogenizer with a tight-fitting pestle (95% of cells were disrupted as detected by Trypan blue staining). Crude lysates were centrifuged at 1,000g for 15 min at 4°C to remove nuclei and unbroken cells in the resulting pellet (P1). The low-speed supernatant was collected and then subjected to a 10,000g centrifugation for 15 min, yielding the 10,000g pellet (P2, containing mitochondria and heavy ER). The supernatant from the P2 pellet was centrifuged at 15,000g in order to remove any remaining mitochondria. Finally, the 15,000g supernatant was separated into cytosol (S3) and light membrane (P3, light ER) fractions by centrifugation at 100,000g for 1 h. The 100,000g supernatant was collected as the S3 fraction and the pellet was resuspended in 60 μl of buffer A. The P2 fraction was washed twice by resuspending cells in 100 μl buffer A and pelleting (10,000g for 15 min). After the final wash, the P2 fraction was resuspended in 60 μl buffer A. The protein content in each fraction (P2, S3, P3) was measured with the bicinchoninic acid method.

Gel Electrophoresis and Western Blotting

Protein samples and pre-stained molecular mass markers (Bio-Rad, Hercules, CA) were denatured in SDS reducing 5X sample buffer and boiled at 90°C for 5 min before gel electrophoresis. The protein samples (40–100 μg/lane) were loaded and separated by SDS-PAGE (4–15% gradient gel or 10% gel). After transferring to a nitrocellulose membrane, the blots were blocked in 7.5% nonfat dry milk in Tris-buffered saline (TBS) for 2 h at room temperature and then incubated with a primary antibody at 4°C overnight. After rinsing, the blots were incubated with horseradish peroxidase-conjugated secondary IgG for 1.5 h at room temperature. Bound antibody was visualized using the enhanced chemiluminescence assay (Amersham Corp, Piscataway, NJ). Relative changes in protein expression were estimated from the integrated pixel intensity of each protein band using Image J software. Mouse anti-Cyt *c* monoclonal antibody (clone 7H8.2C12) (1:800), rabbit anti-IP_3R1 antiserum (1:1000), rabbit anti-MnSOD polyclonal antibody (mitochondria marker, 1:2000), rabbit anti-Calnexin (CNX) polyclonal antibody (microsomal constituent marker, 1:1000),

rabbit anti- the alpha subunit of eukaryotic initiation factor 2 (p-eIF2α) polyclonal antibody (1:500), and mouse anti-actin monoclonal antibody (1:3000) were used.

Statistics

Throughout the study, n values represented the number of cultures used in each experiment. Standard error of mean values for each experimental group was reported as a gauge of the accuracy of the calculated mean. For western blotting assay, standard deviation was reported in the summary data. Statistical significance was determined by either Student's *t*-test or an ANOVA (Bonferroni post-hoc test) for multiple comparisons at a confidence of 95% ($p < 0.05$).

RESULTS

Release of Cyt c from mitochondria in astrocytes following *in vitro* ischemia

Normoxic control astrocytes had a punctate perinuclear pattern of Cyt *c* expression (Figure 1A). Cyt *c* signals were colocalized with immunostaining of mitochondrial protein Mn-superoxide dismutase (MnSOD) (**thin arrow,** Figure 1A). At 60 min REOX following 2 h OGD, mitochondria were swollen (*, Figure 1B) with punctate Cyt *c* distribution. By 160 min REOX, in some astrocytes, Cyt *c* immunostaining was absent and only MnSOD immunoreactive signals were detected in mitochondria (**arrowhead,** Figure 1C). Moreover, Cyt *c* immunoreactivity was enhanced in other astrocytes in which MnSOD immunostaining signals were clearly not colocalized with Cyt *c* (Figure 1C, **thick arrow**). In contrast, in astrocytes treated with 10 μM bumetanide, a potent inhibitor of NKCC1, the Cyt *c* release at 160 min REOX was absent (Figure 1D, thin arrow) and accompanied with less mitochondrial swelling. Similar to the bumetanide-treated astrocytes, $NKCC1^{-/-}$ astrocytes exhibited more resistance to the OGD/REOX-mediated mitochondrial damage. No detectable Cyt *c* release at 160 min REOX was observed in $NKCC1^{-/-}$ astrocytes (Figure 1E, thin arrow). In a positive control study for Cyt *c* release, 10 μM FCCP exposure (4 min) triggered mitochondrial swelling and non-colocalization of Cyt *c* and MnSOD (Figure 1F, arrowhead, thick arrow), which is similar to the ischemic astrocytes.

Quantitative analysis of Cyt *c* release in astrocytes

As shown in Figure 1G, the Rp was 0.65 ± 0.02 and the M2 was 0.72 ± 0.02 in the normoxic control astrocytes, reflecting the relative co-localization of Cyt *c* and MnSOD under this condition. At 60 min REOX when there was moderate Cyt c release, Rp was reduced to 0.53 ± 0.07 and M2 dropped to 0.49 ± 0.03 ($p < 0.05$). Moreover, when Cyt *c* and MnSOD became non-colocalized at 160 min REOX, Rp decreased further to 0.25 ± 0.04 ($p < 0.05$), accompanied with a deep drop in the M2 value (0.20 ± 0.05, $p < 0.05$). Interestingly, cells treated with 10 μM bumetanide or cells from $NKCC1^{-/-}$ mice exhibited significantly less reduction in Rp and M2 values at 160 min REOX ($p < 0.05$). On the other hand, in cells where Cyt *c* release was triggered with 10 μM FCCP, Rp and M2 values were significantly reduced ($p < 0.05$), similar to those at 160 min REOX.

To further investigate the role of ionic dysregulation in OGD/REOX-induced Cyt *c* release from mitochondria, we used SEA0400, a selective inhibitor of NCX_{rev} activity. In astrocytes treated with the NCX_{rev} inhibitor SEA0400 (1 μM) during REOX, the Cyt *c* release at 160 min REOX was absent (**data not shown**). The summary data in Figure 1G illustrate that cells treated with SEA0400 did not exhibit significant reduction in Rp (0.59 ± 0.02) and in M2 values (0.65 ± 0.01) at 160 min REOX. This was in contrast to the low Rp (0.25 ± 0.04) and M2 (0.20 ± 0.05) values in the 160 min REOX groups. These data further demonstrates a role for NCX_{rev} in mitochondrial damage in ischemic astrocytes.

Colocalization of Cyt *c* and MnSOD in astrocytes was further analyzed by plotting the distribution of Rp and M2 values. The majority of normoxic control astrocytes exhibited high Rp or M2 values with a normal distribution (Kolmogorov-Smirnov normality test, $p > 0.2$, Suppl. Figure 1 A, C). In contrast, following 2 h OGD/160 min REOX, the number of astrocytes with low Rp or M2 values were increased and the cell distribution drastically shifted to the left part of the x-axis (Suppl. Figure 1 A, C). Moreover, the OGD/REOX-treated cells were not normally distributed (Kolmogorov-Smirnov normality test, $p < 0.05$). On the other hand, either pharmacological inhibition of NKCC1 with bumetanide or genetic ablation prevented the Cyt *c* release. Cells maintained a normal distribution pattern with high values of Rp or M2 (Suppl. Figure 1 B, D). Taken together, these analyses clearly demonstrate a release of Cyt *c* from mitochondria in astrocytes following OGD/REOX, and the protective effects of NKCC1 inhibition with bumetanide or by genetic ablation.

Delayed elevation in $[Ca^{2+}]_{cyt}$ following OGD/REOX

We investigated the time course of changes in $[Ca^{2+}]_{cyt}$ following OGD/REOX. As shown in Figure 2A, there were no changes in $[Ca^{2+}]_{cyt}$ after 2 h OGD. Interestingly, $[Ca^{2+}]_{cyt}$ started to rise at ~ 120 min REOX at a rate of ~ 8 nM/min and reached a plateau (358 ± 25 nM) between 160–180 min REOX. Moreover, the timing of the $Ca^{2+}{}_{cyt}$ increase was close to the release of significant Cyt *c* at 160 min REOX. In contrast, inhibition of NKCC1 activity with bumetanide abolished the delayed rise in $[Ca^{2+}]_{cyt}$ (Figure 2B). To test the role of NCX_{rev} in delayed Ca^{2+} dysregulation, we examined whether SEA0400 (1μM), a potent inhibitor of NCX_{rev}, can block Ca^{2+} rise during OGD/REOX. Inhibition of NCX_{rev} prevented the delayed rise in $[Ca^{2+}]_{cyt}$ (Figure 2B), which is similar to the effects of NKCC1 inhibition.

We speculated that the delayed elevation of $[Ca^{2+}]_{cyt}$ may result from IP_3R-mediated Ca^{2+} release from ER. As shown in Figure 2C, inhibition of IP_3R with its specific inhibitor xestospongin C (20 μM) largely blocked the delayed rise in $[Ca^{2+}]_{cyt}$, suggesting ER Ca^{2+} stores as the source for the post-OGD Ca^{2+} rise in the cytosol. Moreover, we observed a sudden loss of fura-2 fluorescence signal in some astrocytes during 120–180 min REOX (Figure 2 D-left panel, arrow). These dying cells with damaged membrane integrity failed to retain the dye. As shown **in the lower panel** of Figure 2 D-right panel, normoxic astrocytes exhibited a basal level of cell death (6% ± 2 %). In contrast, 24 ± 3 % astrocytes died during 180 min REOX following 2 h OGD. Most importantly, a time-dependent cell death analysis revealed that the majority of cell death occurred during 125–180 min REOX, when the cytosolic Ca^{2+} dysregulation was triggered (Suppl. Figure 2). Inhibition of NKCC1 or NCX_{rev} activity with Bu or SEA0400 prevented the OGD/REOX-induced astrocyte cell death (Figure 2D).

Biphasic changes in $[Ca^{2+}]_{ER}$ and $Ca^{2+}{}_{m}$ following OGD/REOX

The delayed rise in $[Ca^{2+}]_{cyt}$ may result from the release of $Ca^{2+}{}_{ER}$. To test this hypothesis, changes of $[Ca^{2+}]_{ER}$ were determined. Figure 3A shows that $[Ca^{2+}]_{ER}$ was increased from a resting level of 27 ± 3 μM to 65 ± 3 μM at 2 h OGD ($p < 0.05$). During REOX, $[Ca^{2+}]_{ER}$ was further augmented and reached a peak value of 130 ± 2 μM by 90 min REOX. However, after ~ 90 min REOX, $Ca^{2+}{}_{ER}$ was abruptly released, occurring at the time when $[Ca^{2+}]_{cyt}$ was increasing. $Ca^{2+}{}_{ER}$ appeared to start refilling at 3 h REOX. These findings demonstrate that OGD/REOX causes $Ca^{2+}{}_{ER}$ biphasic dysregulation in astrocytes. The release of $Ca^{2+}{}_{ER}$ may in part contribute to the detrimental delayed increase in $Ca^{2+}{}_{cyt}$.

Consistent with its effect on $[Ca^{2+}]_{cyt}$, inhibition of NKCC1 activity with bumetanide during REOX not only significantly attenuated REOX-mediated augmentation of $Ca^{2+}{}_{ER}$ loading, but also blocked REOX-triggered $Ca^{2+}{}_{ER}$ release (Figure 3A). To investigate whether IP_3R

plays a role in Ca^{2+}_{ER} release, inhibition of IP_3R with a non-selective inhibitor 2-APB (100 μM) was tested. As shown in Figure 3B, 2-APB did not significantly affect accumulation of Ca^{2+}_{ER} during 0–90 min REOX, but it reduced the release of Ca^{2+}_{ER} during 2–3 h REOX. To further confirm the role of the IP_3R in the OGD/REOX-mediated release of Ca^{2+}_{ER}, we also used the specific IP_3R blocker xestospongin C (20 μM). The presence of xestospongin C during OGD/REOX did not affect Ca^{2+}_{ER} accumulation at 90 min REOX, but it did prevent depletion of Ca^{2+}_{ER} stores at 160 min REOX (Figure 3B). Taken together, these data suggest that REOX-triggered Ca^{2+}_{ER} release is in part due to IP_3R activation.

To further investigate whether REOX-triggered Ca^{2+}_{ER} release would affect mitochondrial Ca^{2+} homeostasis and mitochondrial function, we next monitored the relative change in the rhod-2 florescence in mitochondria following 2 h OGD. Three hours of normoxic perfusion did not result in significant changes in Ca^{2+}_{m} (Figure 3C). However, within 15 min of REOX following 2 h OGD, there was a significant increase in Ca^{2+}_{m} that reached a plateau by 30 min REOX (~ 3-fold, Figure 3C). Interestingly, there was a second increase in Ca^{2+}_{m} between 90–120 min of REOX, when Ca^{2+}_{ER} release and increases in $[Ca^{2+}]_{cyt}$ occurred. Inhibition of NKCC1 either with bumetanide or by genetic ablation did not prevent the initial post-OGD loading of Ca^{2+}_{m}, but completely blocked the secondary rise in Ca^{2+}_{m} (Figure 3C). Interestingly, inhibition of IP_3R with xestospongin C also abolished the second phase increase in Ca^{2+}_{m}, implying that the source for this second Ca^{2+}_{m} rise is ER (Figure 3D). Taken together, the data suggest that the OGD/REOX-induced released of Ca^{2+}_{ER} is partially buffered by mitochondria and this may facilitate mitochondrial Cyt *c* release.

Translocation of Cyt *c* from mitochondria to ER at 160 min REOX

Translocation of Cyt *c* into ER may play a role in IP_3R activation and Ca^{2+}_{ER} release. We measured relative changes of Cyt *c* content in different subcellular fractionations (mitochondria and heavy endoplasmic reticulum; cytosol; and endoplasmic reticulum) following OGD/REOX. Figure 4A shows that the cytosol fraction lacked mitochondrial MnSOD and ER marker protein calnexin (CNX) expression. No MnSOD was detected in ER fraction (P3). Thus, relatively pure cytosol and ER fractions were obtained in this study. However, the P2 fraction (mitochondria and heavy endoplasmic reticulum) contained both MnSOD and CNX. The impurity of mitochondrial fraction is less relevant to this study, because our focus is on Cyt *c* translocation to the ER fraction (P3).

Under normoxic control conditions, Cyt *c* was largely located in mitochondria and only a trace level of Cyt *c* was detected in ER fraction (Figure 4A). At 120 min REOX after 2 h OGD, the Cyt *c* level in ER was elevated and further increased by 160 min REOX. The Cyt *c*/CNX ratio was increased by ~ 2-fold at 160 min REOX (Figure 4B). Moreover, inhibition of NKCC1 with 10 μM bumetanide significantly reduced the amount of Cyt *c* translocated to ER fraction at 160 min REOX ($p < 0.05$).

Changes of ER stress protein following OGD/REOX

Ca^{2+}_{ER} dysregulation can lead to the unfolded protein response and ER stress development (Groenendyk and Michalak 2005). We examined whether expression of ER stress proteins such as the phosphorylated form of eIF2α (p-eIF2α) was altered. As shown in Figure 5A, expression of p-eIF2α protein was increased at 2 h OGD and reached a peak level (~3.5-fold) at 120 min REOX ($p < 0.05$), when ER Ca^{2+} depletion occurred. p-eIF2α remained elevated at 3 h REOX. Inhibition of NKCC1 activity with bumetanide during 0–3 h REOX attenuated the up-regulation of p-eIF2α protein (Figure 5B). These results imply that Ca^{2+}_{ER} dysregulation was accompanied by transient ER unfolded protein responses during 2 h OGD and 0–3 h REOX.

DISCUSSION

OGD/REOX disrupts ER Ca^{2+} store homeostasis

In this study, we found that 2 h of OGD led to an ~2.4 fold Ca^{2+} accumulation in ER stores. During REOX, Ca^{2+}_{ER} continued to rise until an abrupt release of ER Ca^{2+} occurred between 90–160 min REOX. Interestingly, the release of Ca^{2+} from ER stores was accompanied by a delayed rise in Ca^{2+}_{cyt}. These findings demonstrate that astrocyte ER Ca^{2+} stores buffer cytosolic Ca^{2+} in an attempt to maintain cytosolic Ca^{2+} homeostasis following OGD/REOX. An increase in IP_3R-sensitive ER Ca^{2+} stores has been revealed in astrocytes under conditions of Na^+/K^+ ATPase inhibition or chronic hypoxia (Golovina and Blaustein 2000; Smith et al. 2003). The absence of detectable increases in Ca^{2+}_{cyt} during early REOX suggests that ER is located near the sites of Ca^{2+} influx across the plasma membrane and facilitates Ca^{2+} uptake into ER stores. Indeed, it has been reported that NCX-1 and Na^+/K^+ ATPase are co-distributed in the plasma membrane regions of smooth muscle and are also in register with the sarcoplasmic reticulum (Moore et al. 1993). Furthermore, Goldman et al. showed that when NCX_{rev} is stimulated by application of ouabain and reduction of extracellular Na^+, NCX_{rev}-induced increases in Ca^{2+}_{cyt} can be buffered by ER (Goldman et al. 1994). Our findings further indicate that excessive Ca^{2+} influx via stimulation of NCX_{rev} in ischemic astrocytes can be rapidly taken up by ER.

Here we report first-line evidence that astrocytes deplete ER Ca^{2+} stores in an *in vitro* model of ischemia. The release of Ca^{2+} from ER stores between 90 –160 min of REOX was associated with the loss of Ca^{2+}_{cyt} homeostasis as well as with a secondary increase in Ca^{2+}_{m} and the release of Cyt *c* from mitochondria. Interestingly, depletion of ER Ca^{2+} stores was muted by both non-specific (2-APB) and specific (xestospongin C) inhibitors of IP_3R, suggesting a primary role for IP_3R in the ER Ca^{2+} depletion in astrocytes. Both global or focal cerebral ischemia cause hydrolysis of poly-PI and formation of IP_3 through activation of PLC (Lin et al. 1991; Yoshida et al. 1986). Group I metabotropic glutamate receptor (mGluR) stimulates poly-PI turnover and therefore can influence IP_3 levels (Conn and Pin 1997). Activation of mGluR5 has been shown to trigger a sustained astrocyte Ca^{2+} oscillation in the ischemic core and penumbra following photothrombosis ischemia, in part due to IP_3-induced Ca^{2+} release (Ding et al. 2009; Bruno et al. 2001). Our findings further suggest that IP_3R-mediated ER Ca^{2+} depletion in astrocytes may occur in ischemic brain particularly during the reperfusion period and exacerbate astrocyte damage.

Effects of ER Ca^{2+}depletion on astrocyte function

Loss of Ca^{2+}_{ER} homeostasis can affect many functions of the ER, including changes in protein folding and in ER stress (Orrenius et al. 2003). Depletion of Ca^{2+}_{ER} stores with thapsigargin can lead to ER stress (Paschen and Doutheil 1999) which induces suppression of protein synthesis, polyribosomal disaggregation, and activation of ER stress genes (Doutheil et al. 1997; Mengesdorf et al. 2001). This ER stress response is almost identical to the responses found in transient cerebral ischemia (Althausen et al. 2001; Kumar et al. 2003; DeGracia et al. 1999). Glial degeneration after hypoxia-ischemia or focal ischemia has been detected in immature and mature brains with both apoptotic or necrosis cell death features (Gelot et al. 2009; Giffard and Swanson 2005). The underlying cell damage mechanisms involve activation of caspase-dependent signaling pathways and oxidative stress (Ouyang et al. 2007). In our current study, we observed that OGD/REOX caused a sharp, sustained elevation of ER stress protein p-eIF2α, which was accompanied with dysregulation of ER Ca^{2+} and ~ 25% cell death. This suggests that ER Ca^{2+} dysregulation and ER stress may also contribute to astrocyte demise in ischemic brains. Future experiments should include investigating whether these changes occur in reactive astrocytes in *in vivo* ischemic brains.

It is well established that Ca^{2+} transients and/or synchronized Ca^{2+} transients (Ca^{2+} oscillations) represent a form of astrocyte excitability and play an important role in astrocyte-astrocyte as well as in astrocyte-neuron intercellular communication (Koizumi 2010). These regulated increases in astrocyte $[Ca^{2+}]_{cyt}$ can result from release of Ca^{2+} from ER stores and trigger gliotransmitter release (glutamate, purines). Astrocytes respond to hypoxia/ischemia insults by developing reactive astrogliosis, which is reflected by up-regulation of GFAP expression, astrocyte hypertrophy, and proliferation (Xiong et al. 2009; Hwang et al. 2008; Ouyang et al. 2007). Reactive astrocytes change in their ability to release, take up, and metabolize gliotransmitters. Thus, they may cause unusual excitation of adjacent local neuronal networks and participate in pathophysiology of epilepsy after brain injury (Koizumi 2010). In our current study,~ 75% of the astrocytes did not die, but exhibited depletion of $Ca^{2+}{}_{ER}$ and sustained elevation in $[Ca^{2+}]_{cyt}$ following OGD/REOX. If these changes also occur in reactive astrocytes following *in vivo* cerebral ischemia, they may represent the dysfunction of reactive astrocytes and contribute to ischemic brain damage. This speculation requires confirmation in a future study.

Mitochondrial dysfunction following OGD/REOX

In our study, longer REOX periods (90–160 min REOX) resulted in secondary increases in $Ca^{2+}{}_{m}$. Interestingly, the secondary increase in $Ca^{2+}{}_{m}$ occurred in the same time period when $Ca^{2+}{}_{ER}$ release and $[Ca^{2+}]_{cyt}$ were elevated. Increases in $Ca^{2+}{}_{m}$ can directly induce formation of the mitochondrial permeability transition pore (PTP) in the inner mitochondrial membrane (Ichas et al. 1997) and cause the depolarization of the mitochondrial membrane potential. Reichert and colleagues reported that inhibition of PTP by cyclosporin A could prevent loss of mitochondrial membrane potential in astrocytes and block the subsequent Cyt *c* release triggered by 45–60 min of OGD (Reichert et al. 2001).

In our current study, we found that 120 min REOX following 2 h OGD triggered Cyt *c* translocation from mitochondrial fraction to ER fraction. The amount of Cyt *c* translocated to ER increased further at 160 min REOX. One possible explanation for the translocation of Cyt *c* to ER is the close physical association or “privileged communication” between ER and mitochondria (Rizzuto et al. 1998). The lack of significant Cyt *c* accumulation in cytosol has been reported in astrocytes after OGD/REOX (Reichert et al. 2001), which has been attributed to rapid modification and/or degradation of Cyt *c* after its release from mitochondria. It should be noted that in the current study, we consistently observed abundant Cyt *c* signals in the mitochondrial fraction (regardless of experimental conditions) as assayed by the immunoblotting, compared to the immunostaining data. This discrepancy may in part be attributed to the epitope of Cyt *c* being readily exposed under the denatured conditions of immunoblotting, thereby enhancing the antibody binding.

We hypothesized that the released Cyt *c* binds to IP_3R in ER and facilitate $Ca^{2+}{}_{ER}$ release. Cyt *c* binding to the C terminus of IP_3R1 has been confirmed in yeast 2-hybrid analysis *in vitro* and in HeLa and PC12 cell lines (Boehning et al. 2003). Furthermore, the binding of Cyt *c* to IP_3R1, as well as to ryanodine receptor type 2, was detected in gerbil hippocampus following transient brain ischemia (Beresewicz et al. 2006). However, recent studies suggest that IP_3R2 plays an important role in ER Ca^{2+} release in cortical and hippocampal astrocytes (Sheppard et al. 1997; Petravicz et al. 2008). Future studies are required to determine whether the released Cyt *c* binds to IP_3R1 or IP_3R2 in astrocytes following OGD/REOX and whether it enhances $Ca^{2+}{}_{ER}$ release.

In the current study, we also observed that the NKCC1 inhibitor bumetanide significantly blocked the secondary increase in $Ca^{2+}{}_{m}$, release of $Ca^{2+}{}_{ER}$ and Cyt *c*. NKCC1 activity following OGD leads to intracellular Na^{+} overload that stimulates Ca^{2+} entry via NCX_{rev} (Kintner 2007). Inhibition of NCX_{rev} activity by SEA0400 abolished the Cyt *c* release in the

current study. These results imply thatNKCC1 coupled with NCX_{rev} play a role in promoting influx of Ca^{2+} following OGD/REOX, which may eventually overwhelm the buffering capacity of ER and mitochondria and triggers Cyt *c* release and the collapse of mitochondrial function.

In summary, we report here that 2 h OGD/0–3 h REOX triggered biphasic changes of Ca^{2+}_{ER} and a delayed increase of Ca^{2+}_{cyt} and Ca^{2+}_{m} in astrocytes. The abrupt Ca^{2+}_{ER} release during 90–160 min was accompanied with a second rise of Ca^{2+}_{m} and a profound Cyt *c* release from mitochondria. The translocation of Cyt *c* to ER may enhance IP_3R-dependent Ca^{2+}_{ER} release. Interestingly, inhibition of ion transporters such as NKCC1 and NCX_{rev} prevented many of these changes. Taken together, the coupling of Ca^{2+} ER signaling and mitochondrial dysfunction may play an important role in astrocyte damage following ischemia.

Supplementary Material

Refer to Web version on PubMed Central for supplementary material.

Acknowledgments

This work was supported in part by an NIH grant R01NS38118 and AHA EIA 0540154 (D. Sun), NIH grant P30 HD03352 (Waisman Center), an NIH grant R01HL61974 (G. E. Shull), and China Scholarship Council Postgraduate Scholarship Program (Y. Liu).

ABBREVIATIONS

Bu	bumetanide
dBcAMP	dibutyryl cyclic AMP
$[Ca^{2+}]_{cyt}$	calcium concentration cytoplasmic
$[Ca^{2+}]_{ER}$	calcium concentration endoplasmic reticulum
Ca^{2+}_{m}	mitochondrial calcium
CNX	calnexin
Cyt *c*	cytochrome *c*
DIV	days in culture
ER	endoplasmatic reticulum
FBS	fetal bovine serum
FCCP	carbonyl cyanide-p-trifluoromethoxyphenylhydrazone
Fura-2 AM	Fura-2 acetoxymethyl ester
HBSS	Hanks balanced salt solution
IP_3R	inositol 1,4,5-triphosphate receptor
M2	Manders' coefficient
Ψ_m	mitochondrial membrane potential
mGluR	Group I metabotropic glutamate receptor
MnSOD	manganese superoxide dismutase
NCX_{rev}	reverse mode function of Na^+/Ca^{2+} exchanger

NKCC1	Na^+-K^+-Cl^- cotransporter isoform 1
OGD/REOX	oxygen glucose deprivation and reoxygenation
p-eIF2α	phosphorylated eukaryotic initiation factor 2 alpha
PTP	mitochondrial permeability transition pore
Rp	Pearson's coefficient
RyR_2	ryanodine receptor type 2
XeC	xestospongin C

References

Althausen S, Mengesdorf T, Mies G, Olah L, Nairn AC, Proud CG, Paschen W. Changes in the phosphorylation of initiation factor eIF-2 alpha, elongation factor eEF-2 and p70 S6 kinase after transient focal cerebral ischaemia in mice. J Neurochem. 2001; 78:779–787. [PubMed: 11520898]

Beresewicz M, Kowalczyk JE, Zablocka B. Cytochrome c binds to inositol (1,4,5) trisphosphate and ryanodine receptors in vivo after transient brain ischemia in gerbils. Neurochem Int. 2006; 48:568–571. [PubMed: 16513219]

Boehning D, Patterson RL, Sedaghat L, Glebova NO, Kurosaki T, Snyder SH. Cytochrome c binds to inositol (1,4,5) trisphosphate receptors, amplifying calcium-dependent apoptosis. Nat Cell Biol. 2003; 5:1051–1061. [PubMed: 14608362]

Boehning D, Patterson RL, Snyder SH. Apoptosis and calcium: new roles for cytochrome c and inositol 1,4,5-trisphosphate. Cell Cycle. 2004; 3:252–254. [PubMed: 14726673]

Bolte S, Cordelieres FP. A guided tour into subcellular colocalization analysis in light microscopy. J Microsc. 2006; 224:213–232. [PubMed: 17210054]

Bondarenko A, Svichar N, Chesler M. Role of Na^+-H^+ and Na^+-Ca^{2+} exchange in hypoxia-related acute astrocyte death. Glia. 2005; 49:143–152. [PubMed: 15390092]

Bruno V, Battaglia G, Copani A, D'Onofrio M, Di Iorio P, De Blasi A, Melchiorri D, Flor PJ, Nicoletti F. Metabotropic glutamate receptor subtypes as targets for neuroprotective drugs. J Cereb Blood Flow Metab. 2001; 21:1013–1033. [PubMed: 11524608]

Chen X, Kintner DB, Luo J, Baba A, Matsuda T, Sun D. Endoplasmic reticulum Ca^{2+} dysregulation and endoplasmic reticulum stress following in vitro neuronal ischemia: role of Na^+-K^+-Cl^- cotransporter. J Neurochem. 2008; 106:1563–1576. [PubMed: 18507737]

Conn PJ, Pin JP. Pharmacology and functions of metabotropic glutamate receptors. Annu Rev Pharmacol Toxicol. 1997; 37:205–237. [PubMed: 9131252]

DeGracia DJ, Adamczyk S, Folbe AJ, et al. Eukaryotic initiation factor 2 alpha kinase and phosphatase activity during postischemic brain reperfusion. Exp Neurol. 1999; 155:221–227. [PubMed: 10072297]

Ding S, Wang T, Cui W, Haydon PG. Photothrombosis ischemia stimulates a sustained astrocytic Ca^{2+} signaling in vivo. Glia. 2009; 57:767–776. [PubMed: 18985731]

Doutheil J, Gissel C, Oschlies U, Hossmann KA, Paschen W. Relation of neuronal endoplasmic reticulum calcium homeostasis to ribosomal aggregation and protein synthesis: implications for stress-induced suppression of protein synthesis. Brain Res. 1997; 775:43–51. [PubMed: 9439827]

Flagella M, Clarke LL, Miller ML, et al. Mice lacking the basolateral Na-K-2Cl cotransporter have impaired epithelial chloride secretion and are profoundly deaf. J Biol Chem. 1999; 274:26946–26955. [PubMed: 10480906]

Gelot A, Villapol S, Billette dV, Renolleau S, Charriaut-Marlangue C. Astrocytic demise in the developing rat and human brain after hypoxic-ischemic damage. Dev Neurosci. 2009; 31:459–470. [PubMed: 19672074]

Giffard RG, Swanson RA. Ischemia-induced programmed cell death in astrocytes. Glia. 2005; 50:299–306. [PubMed: 15846803]

Goldman WF, Yarowsky PJ, Juhaszova M, Krueger BK, Blaustein MP. Sodium/calcium exchange in rat cortical astrocytes. J Neurosci. 1994; 14:5834–5843. [PubMed: 7523629]

Golovina VA, Blaustein MP. Unloading and refilling of two classes of spatially resolved endoplasmic reticulum Ca^{2+} stores in astrocytes. Glia. 2000; 31:15–28. [PubMed: 10816603]

Groenendyk J, Michalak M. Endoplasmic reticulum quality control and apoptosis. Acta Biochim Pol. 2005; 52:381–395. [PubMed: 15933766]

Hwang IK, Yoo KY, An SJ, et al. Late expression of Na^+/H^+ exchanger 1 (NHE1) and neuroprotective effects of NHE inhibitor in the gerbil hippocampal CA1 region induced by transient ischemia. Exp Neurol. 2008; 212:314–323. [PubMed: 18511042]

Ichas F, Jouaville LS, Mazat JP. Mitochondria are excitable organelles capable of generating and conveying electrical and calcium signals. Cell. 1997; 89:1145–1153. [PubMed: 9215636]

Kintner DB, Luo J, Gerdts J, Ballard AJ, Shull GE, Sun D. Role of Na^+-K^+-Cl^- cotransport and Na^+/Ca^{2+} exchange in mitochondrial dysfunction in astrocytes following in vitro ischemia. Am J Physiol Cell Physiol. 2007; 292:C1113–C1122. [PubMed: 17035299]

Koizumi S. Synchronization of Ca^{2+} oscillations: involvement of ATP release in astrocytes. FEBS J. 2010; 277:286–292. [PubMed: 19895581]

Kumar R, Krause GS, Yoshida H, Mori K, DeGracia DJ. Dysfunction of the unfolded protein response during global brain ischemia and reperfusion. J Cereb Blood Flow Metab. 2003; 23:462–471. [PubMed: 12679723]

Lenart B, Kintner DB, Shull GE, Sun D. Na-K-Cl cotransporter-mediated intracellular Na^+ accumulation affects Ca^{2+} signaling in astrocytes in an in vitro ischemic model. J Neurosci. 2004; 24:9585–9597. [PubMed: 15509746]

Lin TN, Liu TH, Xu J, Hsu CY, Sun GY. Brain polyphosphoinositide metabolism during focal ischemia in rat cortex. Stroke. 1991; 22:495–498. [PubMed: 1850877]

Manders EM, Stap J, Brakenhoff GJ, van Driel R, Aten JA. Dynamics of three-dimensional replication patterns during the S-phase, analysed by double labelling of DNA and confocal microscopy. J Cell Sci. 1992; 103:857–862. [PubMed: 1478975]

Marks JD, Boriboun C, Wang J. Mitochondrial nitric oxide mediates decreased vulnerability of hippocampal neurons from immature animals to NMDA. J Neurosci. 2005; 25:6561–6575. [PubMed: 16014717]

Mengesdorf T, Althausen S, Oberndorfer I, Paschen W. Response of neurons to an irreversible inhibition of endoplasmic reticulum Ca^{2+}-ATPase: relationship between global protein synthesis and expression and translation of individual genes. Biochem J. 2001; 356:805–812. [PubMed: 11389688]

Moore ED, Etter EF, Philipson KD, Carrington WA, Fogarty KE, Lifshitz LM, Fay FS. Coupling of the Na^+/Ca^{2+} exchanger, Na^+/K^+ pump and sarcoplasmic reticulum in smooth muscle. Nature. 1993; 365:657–660. [PubMed: 8413629]

Orrenius S, Zhivotovsky B, Nicotera P. Regulation of cell death: the calcium-apoptosis link. Nat Rev Mol Cell Biol. 2003; 4:552–565. [PubMed: 12838338]

Ouyang YB, Voloboueva LA, Xu LJ, Giffard RG. Selective dysfunction of hippocampal CA1 astrocytes contributes to delayed neuronal damage after transient forebrain ischemia. J Neurosci. 2007; 27:4253–4260. [PubMed: 17442809]

Paschen W, Doutheil J. Disturbances of the functioning of endoplasmic reticulum: a key mechanism underlying neuronal cell injury? J Cereb Blood Flow Metab. 1999; 19:1–18. [PubMed: 9886350]

Petravicz J, Fiacco TA, McCarthy KD. Loss of IP3 receptor-dependent Ca^{2+} increases in hippocampal astrocytes does not affect baseline CA1 pyramidal neuron synaptic activity. J Neurosci. 2008; 28:4967–4973. [PubMed: 18463250]

Reichert SA, Kim-Han JS, Dugan LL. The mitochondrial permeability transition pore and nitric oxide synthase mediate early mitochondrial depolarization in astrocytes during oxygen-glucose deprivation. J Neurosci. 2001; 21:6608–6616. [PubMed: 11517250]

Rizzuto R, Pinton P, Carrington W, Fay FS, Fogarty KE, Lifshitz LM, Tuft RA, Pozzan T. Close contacts with the endoplasmic reticulum as determinants of mitochondrial Ca^{2+} responses. Science. 1998; 280:1763–1766. [PubMed: 9624056]

Sheppard CA, Simpson PB, Sharp AH, Nucifora FC, Ross CA, Lange GD, Russell JT. Comparison of type 2 inositol 1,4,5-trisphosphate receptor distribution and subcellular Ca^{2+} release sites that support Ca^{2+} waves in cultured astrocytes. J Neurochem. 1997; 68:2317–2327. [PubMed: 9166724]

Smith IF, Boyle JP, Plant LD, Pearson HA, Peers C. Hypoxic remodeling of Ca^{2+} stores in type I cortical astrocytes. J Biol Chem. 2003; 278:4875–4881. [PubMed: 12477727]

Su G, Kintner DB, Flagella M, Shull GE, Sun D. Astrocytes from Na(+)-K(+)-Cl(−) cotransporter-null mice exhibit absence of swelling and decrease in EAA release. Am J Physiol Cell Physiol. 2002; 282:C1147–C1160. [PubMed: 11940530]

Sun D, Lytle C, O'Donnell ME. Astroglial cell-induced expression of Na-K-Cl cotransporter in brain microvascular endothelial cells. Am J Physiol. 1995; 269:C1506–C1512. [PubMed: 8572180]

Swanson RA, Liu J, Miller JW, Rothstein JD, Farrell K, Stein BA, Longuemare MC. Neuronal regulation of glutamate transporter subtype expression in astrocytes. J Neurosci. 1997; 17:932–940. [PubMed: 8994048]

Takano T, Oberheim N, Cotrina ML, Nedergaard M. Astrocytes and ischemic injury. Stroke. 2009; 40:S8–12. [PubMed: 19064795]

Xiong M, Yang Y, Chen GQ, Zhou WH. Post-ischemic hypothermia for 24h in P7 rats rescues hippocampal neuron: association with decreased astrocyte activation and inflammatory cytokine expression. Brain Res Bull. 2009; 79:351–357. [PubMed: 19406216]

Yoshida S, Ikeda M, Busto R, Santiso M, Martinez E, Ginsberg MD. Cerebral phosphoinositide, triacylglycerol, and energy metabolism in reversible ischemia: origin and fate of free fatty acids. J Neurochem. 1986; 47:744–757. [PubMed: 3016186]

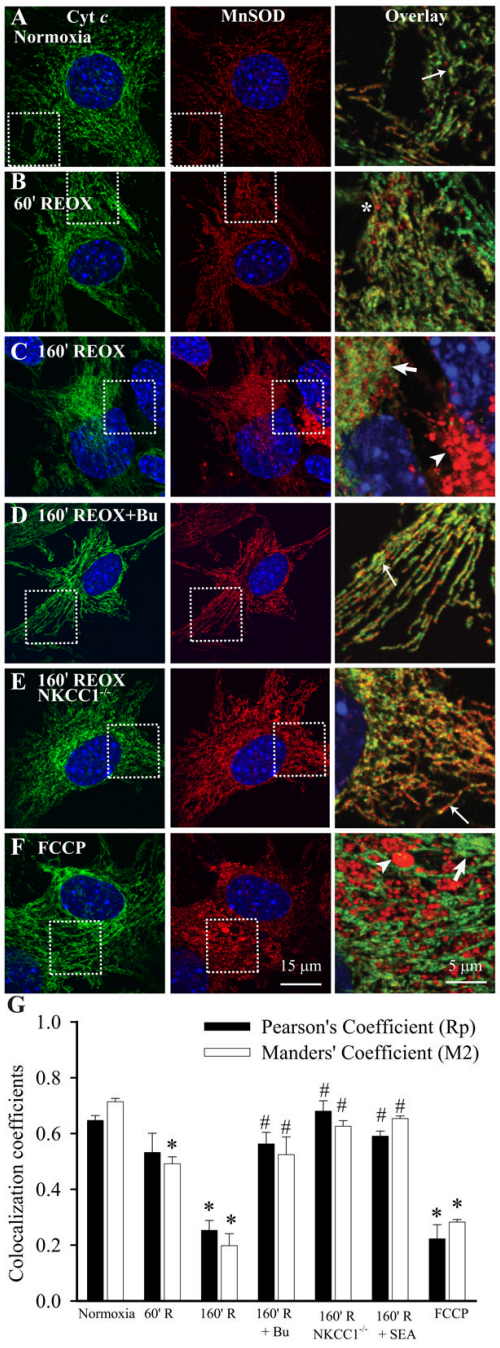

Figure 1. Release of Cyt *c* from mitochondria in astrocytes following OGD/REOX

Localization of Cyt *c* was visualized by staining of astrocytes with an anti-Cyt *c* antibody (green) and with an antibody against the mitochondrial marker protein MnSOD (red). Nuclei were stained with TO-PRO-3 dye (blue). **Overlay:** corresponding Cyt *c* and MnSOD signals in the boxed region (3X magnification). **A**. Normoxic control conditions. **B**. 60 min REOX following 2 h OGD. **C.** 160 min REOX. **D**. 160 min REOX, treated with bumetanide (Bu, 10 μM) during 0–160 min REOX. **E**. Astrocytes from NKCC1$^{-/-}$ mice at 160 min REOX. **F**. Astrocytes treated with 10 μM FCCP for 4 min. ***Thin arrow***: colocalized Cyt *c* and MnSOD signals. ***Thick arrow***: non-colocalized Cyt *c* and MnSOD signals. ***Arrowhead***: cells with MnSOD signals only. *: swollen mitochondria. **G.** Summary data of Rp and M2. The

Cyt *c* release in astrocytes was analyzed with Image J software and the JACop plug-in. In the SEA0400 study, SEA0400 (1 μM) was present during 0–160 min REOX. Data are means ± SEM; n = 3–13. * $p < 0.05$ vs. normoxia; # $p < 0.05$ vs. 160 min REOX.

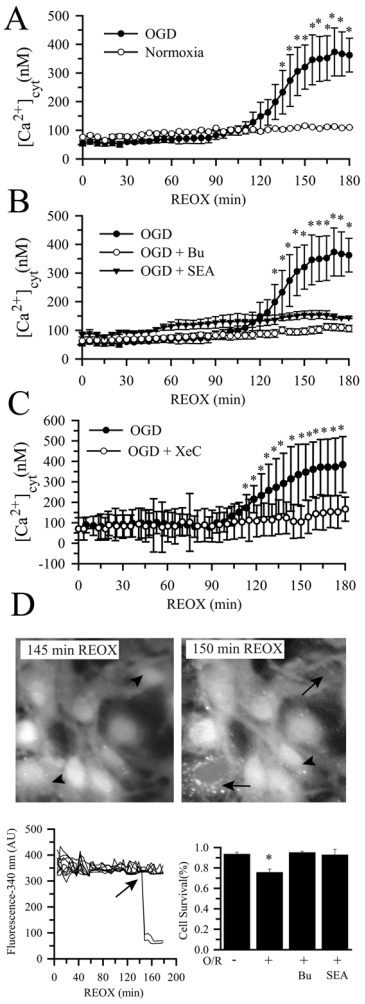

Figure 2. Delayed elevation in $[Ca^{2+}]_{cyt}$ following OGD/REOX

A. $[Ca^{2+}]_{cyt}$ was monitored in single NKCC1$^{+/+}$ astrocytes during 0–180 min REOX following 2 h OGD. Normoxic control were sister NKCC1$^{+/+}$ astrocytes subjected to 3 h normoxic superfusion. **B.** Effects of bumetanide and SEA0400 on $[Ca^{2+}]_{cyt}$. Bumetanide (5 μM) or SEA0400 (1 μM) was present during REOX. Data are means ± SEM; n = 3–4, * $p < 0.05$ vs. normoxia. **C.** Effects of xestospongin C (XeC). Xestospongin C (20μM) was present during REOX only. Data are means ± SD (n = 20 cells). * $p < 0.05$ vs. OGD/REOX + xestospongin C. **D.** Summary data of astrocyte death. **Upper panel**: fura-2 fluorescence in live astrocytes (***arrowhead***) and dying astrocytes (loss of fura-2 signal, ***arrow***). **Lower panels**: sudden loss of fura-2 fluorescence (340 nm wavelength) in dying astrocytes during OGD/REOX (O/R). Data are means ± SEM; n = 3–4, * $p < 0.05$ vs. normoxia.

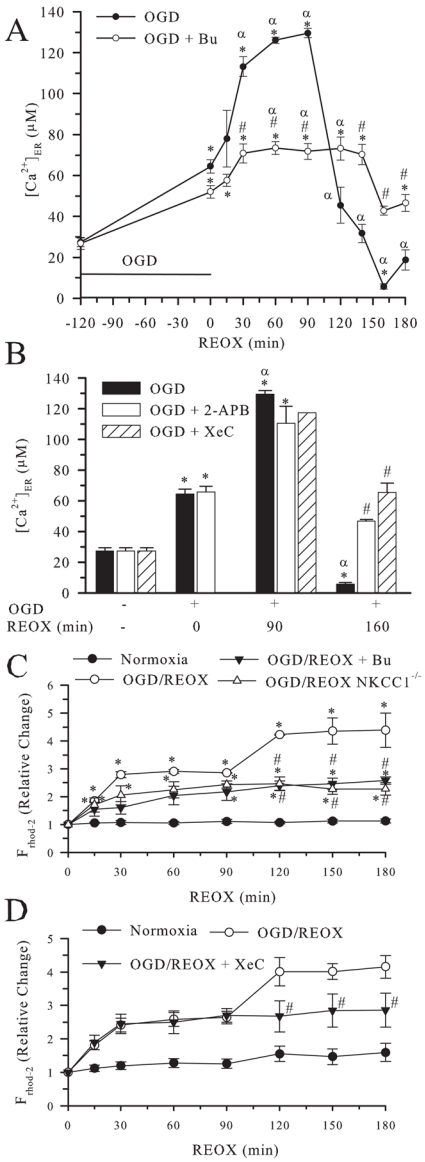

Figure 3. Biphasic changes in $[Ca^{2+}]_{ER}$ and $Ca^{2+}{}_m$ following OGD/REOX

A. $[Ca^{2+}]_{ER}$ was determined in NKCC1$^{+/+}$ astrocytes under normoxic control conditions and at 0–180 min REOX following 2 h OGD. In the bumetanide study, bumetanide (5 μM) was present during REOX. **B.** $[Ca^{2+}]_{ER}$ was determined in NKCC1$^{+/+}$ astrocytes treated with 2-APB, a nonspecific IP_3R inhibitor (100 μM) during 0 min, 90 min, or 160 min REOX, or a specific IP_3R inhibitor xestospongin C (20 μM, XeC). Data are means ± SEM; n = 3–9 (for XeC at 90 min REOX, n = 1). * $p < 0.05$ vs. normoxia, # $p < 0.05$ vs. OGD/REOX untreated; α $p < 0.05$ vs. 0 min REOX. **C**. Relative change in $Ca^{2+}{}_m$ was determined in NKCC1$^{+/+}$ and NKCC1$^{-/-}$ astrocytes under normoxic conditions or at 0–180 min of REOX. Data are means ± SEM; n = 3–5. * $p < 0.05$ vs. normoxia, # $p < 0.05$ vs. OGD/REOX. **D.** Relative change in $Ca^{2+}{}_m$ was determined in NKCC1$^{+/+}$ astrocytes under normoxic conditions or at 0–180 min of REOX. Xestospongin C (XeC, 20 μM) was present during REOX only. Data are means ± SEM; n = 8–35 cells. # $p < 0.05$ vs. OGD/REOX.

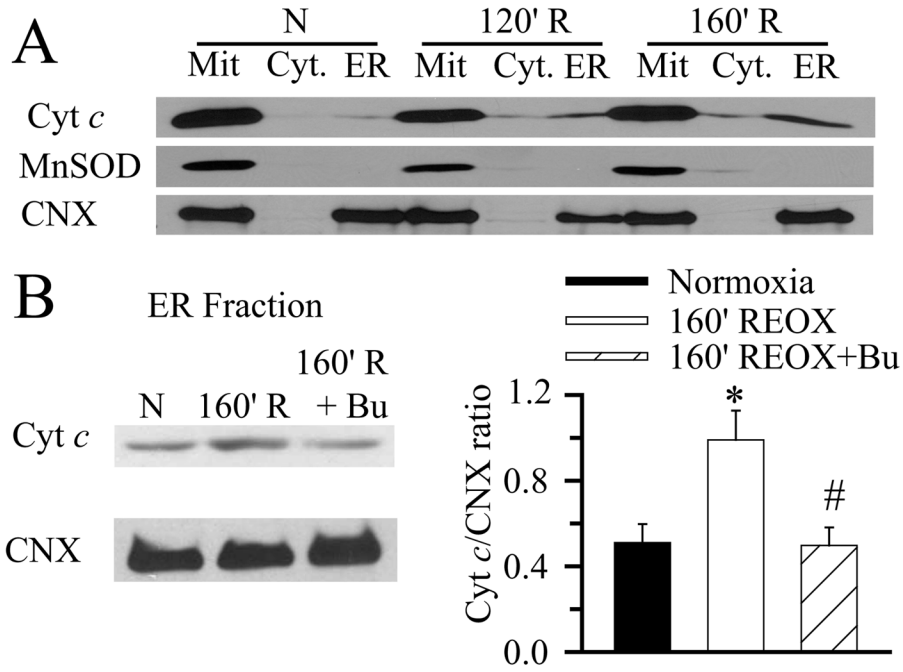

Figure 4. Translocation of Cyt *c* to ER following OGD/REOX

A. Cyt *c* content in mitochondria (P2), cytosol (S3), and ER (P3) fractions was determined. The mitochondrial protein MnSOD and the ER protein calnexin (CNX) were used to determine purity of the fractions and to ensure equal protein loading. 10 μM bumetanide was present during REOX in the drug treated group. **B.** Representative immunoblot of Cyt *c* in ER fraction. CNX on the same blot was probed for sample loading control. Summary data are the ratio of Cyt *c*/CNX intensities. Data are means ± SEM, n = 7. * $p < 0.05$ vs. 160 min REOX.

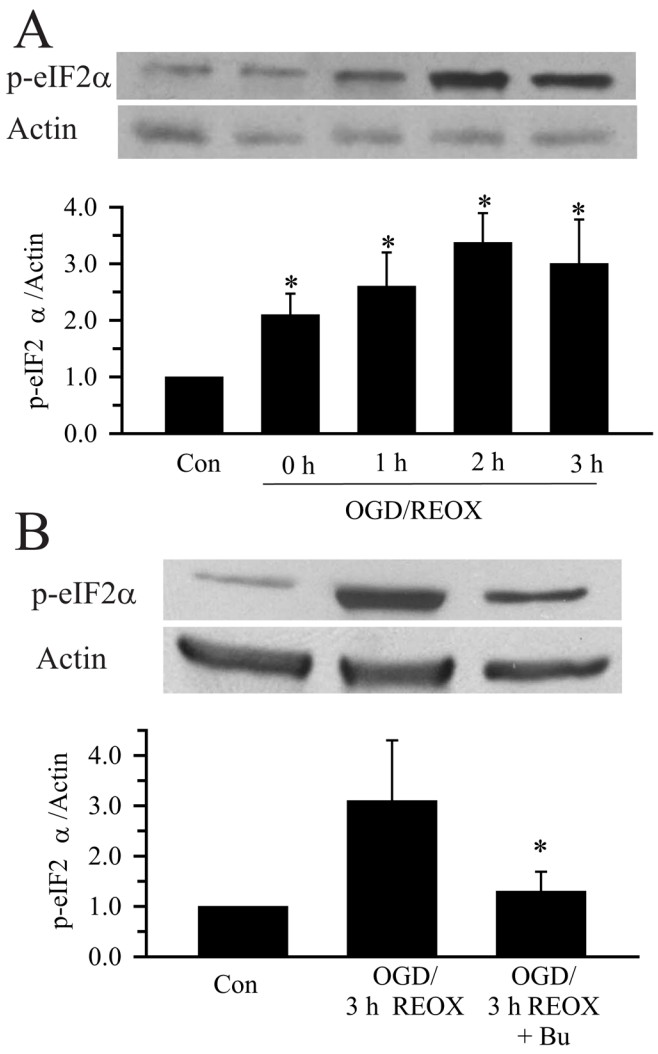

Figure 5. ER stress protein expression

A. OGD/REOX-mediated up-regulation of p-eIF2α. Upper panel: Representative blot showing expression of p-eIF2α protein in normoxic control, 2 h OGD, or 1–3 h REOX. The same blot was probed with anti-actin antibody as a loading control. Lower panel: Summary graph of the relative expression of p-eIF2α protein/actin ratio. Data are means ± SEM. n = 3–4. * $p < 0.05$ vs. Con. **B.** Representative blot showing that the expression of p-eIF2α protein was reduced in astrocytes treated with 10 μM bumetanide during 0–3 h REOX (Upper panel). Lower panel: Summary graph of p-eIF2α protein/actin ratio. Data are means ± SEM n = 3–4. * $p < 0.05$ vs. OGD/REOX.